ACS APPLIED MATERIALS & INTERFACES

Letter

www.acsami.org

Self-Assembled and Highly Selective Sensors Based on Air-Bridge-Structured Nanowire Junction Arrays

Won Jeong Park,[†] Kyung Jin Choi,[†] Myung Hwa Kim,[§] Bon Hyeong Koo,[‡] Jong-Lam Lee,[‡] and Jeong Min Baik*,[†]

[†]School of Mechanical and Advanced Materials Engineering, KIST-UNIST-Ulsan Center for Convergent Materials, Ulsan National Institute of Science and Technology (UNIST), Ulsan, Korea

[§]Department of Chemistry & Nano Science, Ewha Womans University, Seoul, 120-750, Korea

[‡]Department of Materials Science and Engineering, Division of Advanced Materials Science, Pohang University of Science and Technology (POSTECH), Pohang, Gyeongbuk 790-784, Korea

Supporting Information

ABSTRACT: We describe a strategy for creating an air-bridge-structured nanowire junction array platform that capable of reliably discriminating between three gases (hydrogen, carbon monoxide, and nitrogen dioxide) in air. Alternatively driven dual nanowire species of ZnO and CuO with the average diameter of ~30 nm on a single substrate are used and decorated with metallic nanoparticles to form two-dimensional microarray, which do not need to consider the post fabrications. Each individual nanowires in the array form n−n, p−p, and p−n junctions at the micro/nanoscale on single substrate and the junctions act as electrical conducting path for carriers. The adsorption of gas molecules to the surface changes the potential barrier height formed at the junctions and the carrier transport inside the straight semiconductors, which provide the ability of a given sensor array to differentiate among the junctions. The sensors were tested for their ability to distinguish three gases (H_2, CO, and NO_2), which they were able to do unequivocally when the data was classified using linear discriminant analysis.

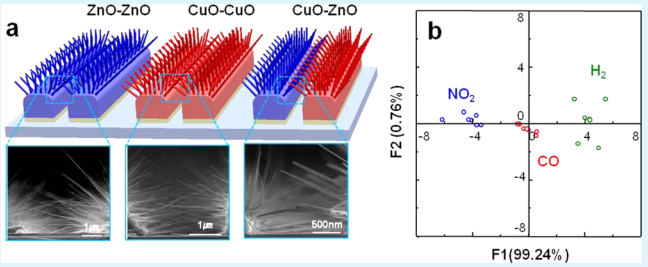

KEYWORDS: *electronic nose (E-nose), metal-oxides, nanowire, copper oxide, zinc oxide, junctions array*

INTRODUCTION

Nanostructured materials such as nanoparticles, nanowires, nanorods, and nanobelts have been extensively studied as building blocks in electronic devices for alternative renewable energy applications and as heterogeneous catalysts because of the modification of their chemical, mechanical, electrical, and optical properties from those of the bulk.[1−4] In particular, because of the very high surface-to-volume ratios, such nanostructures have been used to create very sensitive and selective sensor platforms, named as "electronic nose: e-nose.[5,6] Furthermore, the advent of microelectromechanical systems and nanotechnology have made available new materials platforms, device fabrication alternatives, and novel sensing concept to improve sensitivity, reliability, energy consumption, and response time of the next-generation sensors.[7,8]

In most e-noses, a variety of methods such as different materials and sensor designs (such as temperature gradients) have been employed to differentiate the sensor properties of multicomponent array. Alternatively, the principally different approach is to make sensor arrays based on the semiconductor junctions at the micro/nanoscale, as attractive elements in the potential fabrication of low-power, supersensitive, and rapid response sensors.[9,10] At semiconductor junctions such as n−n and p−n, potential barrier is usually formed because of the depletion region, resulted in rectifying characteristics. The adsorption of gas molecules to the surface changes the potential barrier height at the interface as well as the carrier transport inside the straight semiconductor. Such semiconductor junction sensors based on nanowires and nanoparticles have been successfully demonstrated.[11−13] Recently, sensors based on p-type semiconductors (such as CuO) also has demonstrated considerable potential for the detection of various gases, such as C_2H_5OH, H_2S, H_2, CO, and NH_3.[14−18] Unlike n−n and p−n junctions, the holes in p−p junction flow through the surface accumulation layer, formed near the surface because of the oxygen adsorption when kept in the air.[19]

The adsorbate-induced change of the thickness in hole accumulation layer changes the resistance of the sensors, detecting the gases such as H_2 and C_2H_5OH with high sensitivity and low detection limit.[19,20] The integration of such junctions on a single substrate may thus greatly enhance the selectivity for various gases.

Received: May 2, 2013
Accepted: July 10, 2013
Published: July 10, 2013

dx.doi.org/10.1021/am401635e | ACS Appl. Mater. Interfaces 2013, 5, 6802−6807

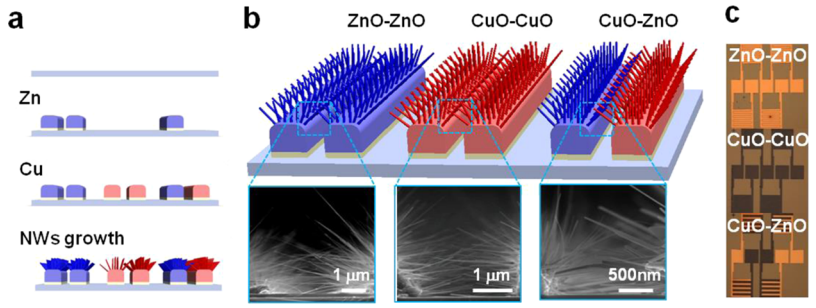

Figure 1. (a) Schematic illustration for alternatively driven metal-oxide nanowires junction. Zn and Cu metal films were selectively deposited by e-beam evaporator, followed by the growth of nanowires on single substrate. (b) Schematic representation of a crossed-nanowire junction array platform and the corresponding SEM images. (c) Optical images of the nanowires junctions on single substrate.

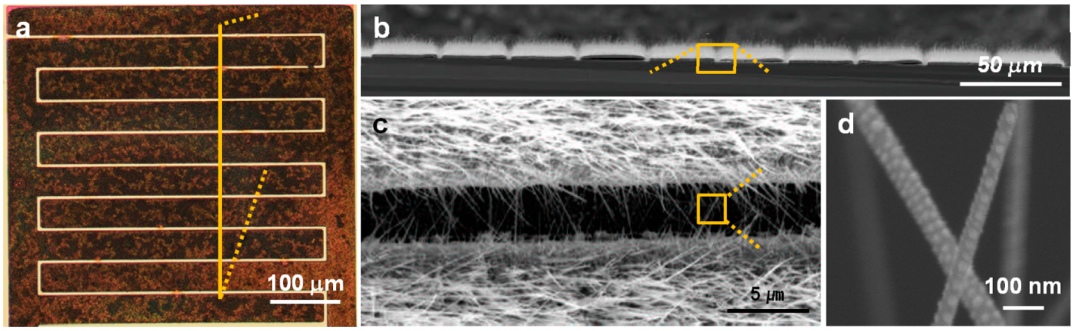

Figure 2. (a) Optical microscope image of junction sensor by the e-beam evaporation which were patterned and separated by the distance of 5 μm via a conventional lithography. (b) Cross-sectional and (c) planar view of SEM images. (d) Enlarged SEM images of the Pd-decorated junction sensor following annealing at 200 °C, the metal films aggregated into well-separated nanoparticles covering the nanowire uniformly.

One issue that impacts on the scale-up of nanosensors is the fact that most nanostructures are fabricated by bottom up technologies which often require the development of post fabrication strategies such as transferring nanowires onto a foreign substrate, orienting nanowires, forming appropriate electrical contacts, and other processes that simultaneously encompass both the micro- and the nanoscales.[21−23] To enhance the orthogonality in responses and enhance the yield in practical multielectrode e-nose systems, it is desirable to integrate one-dimensional (1D) nanostructure with different morphologies and compositions with small dimensions and high surface-to-volume ratios on a single substrate. Here, we describe a strategy for creating an air-bridge-structured percolating nanowire array platform that capable of promptly detecting and reliably discriminating between three gases (hydrogen, carbon monoxide, and nitrogen dioxide) in air[24,25] Alternatively driven dual nanowire species of n-type ZnO and p-type CuO with the average diameter of ∼30 nm on a single substrate is used to form two-dimensional microarray, which do not need to consider the post fabrications. Each individual nanowires in the array form n−n, p−p, and p−n junction in nanoscale on single substrate and the junctions act as electrical conducting path for carriers. The device structure is very simple and efficient compared with those suggested by previous researchers because the electrical contacts to nanowires are self-assembled during the synthesis of nanowires.[26−28] To enhance the sensitivity, palladium (Pd) nanoparticles were decorated on the junction and compared with pristine and Ag-decorated junctions for the capability of e-nose sensors. The Pd and Ag nanoparticles affect the chemistry the surface chemistry occurring on the nanowires and on the metal nanoparticles in two different ways: by the spillover of catalytically produced products on the nanoparticles onto the surface and by creating a charge depletion zone at the Schottky junction formed at the metal/oxides interface, respectively.

EXPERIMENTAL SECTION

Eight-hundred-nanometers-thick Zn and Cu films were deposited on a thermally grown SiO_2 layer with 200 nm thickness on a Si (100) single-crystal substrate by the e-beam evaporation, which were patterned and separated by the distance of 5 μm via a conventional lithography. We adopted an Au electrode (∼200 nm) with Ti adhesion-promotion layer (∼ 20 nm), between the metal films and the substrate. The sample is then transferred to a chemical vapor deposition (CVD) chamber for the growth procedure and heated at 500 °C for 2 h with mixed nitrogen and oxygen (N_2:O_2 = 8:2) flow at 600 Torr. The growth conditions such as temperature, pressure etc. were optimized to obtain the high yields of good-quality nanowires. Two-hour growth at 500 °C typically results in nanowires ∼10 μm in length, long enough to bridge the 5 μm gap between the metal films (see the Supporting Information, Figure S1). At lower temperature (400 °C), the length of ZnO nanowires is not enough to bridge the 5 μm gap between the metal films and they show broad distributions in diameter. Scanning electron microscope (SEM) imaging indicates that in a typical synthesis, the nanowires cover the surface of patterned substrates uniformly and compactly and that the average diameter approximately 30 nm. X-ray diffraction (XRD) analysis of the sample revealed that all of the diffraction peaks could be indexed as a mixture of hexagonal and monoclinic phases, indicating that clearly, the crystal phases of ZnO and CuO are hexagonal and monoclinic phases, without the incorporation of foreign atoms (not shown here).

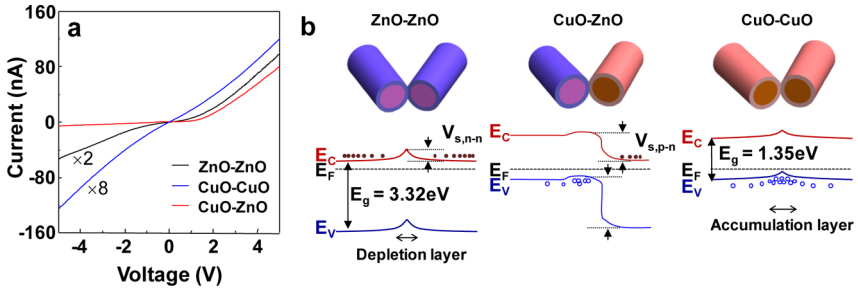

Figure 3. (a) Representative $I-V$ curves measured at room temperature, which show the typical nonlinear Schottky-like transport behaviors. The ×2 and ×8 are 2 times and 8 times of original current, respectively. (b) Energy band diagram of each junction type through the overlapping nanowires. In n−n and p−n junctions, electrons pass over the barrier height, which is strongly dependent on the properties of the contact materials, whereas holes in p−p junction flow through the hole accumulation layer. (The core (dark region) and shell (light region) means the bulk and surface, respectively.)

The overall procedure of the air-bridge-structured percolating nanowires array is shown in Figure 1a. Panels b and c in Figure 1 display many nanowires that bridge across a 5 μm wide gap, forming the nanowire/nanowire junctions that act as electrical conducting path for the carriers. To enhance the sensitivity, we decorated Pd nanoparticles on the junctions using electron beam evaporation at a base pressure of 3.0 × 10^{-6} Torr through a shadow mask, as shown in Figure 2. Following annealing at 200 °C, the metal films aggregated into well-separated nanoparticles covering the nanowire uniformly (Figure 2d). Pristine and Ag-decorated junctions for the capability of e-nose sensors are also prepared on the substrate which Pd-decorated sensors are placed. The sensors were placed in a reaction chamber and exposed to pulses of one of three gases at various partial pressures entrained in flowing dry air with a flow rate of 2000 sccm: H_2 (200 ppm), CO (200 ppm), and NO_2 (200 ppm). The gas sensors were measured in a probe chamber (~125 cm^3) equipped with an electrical measurement system, a vacuum and temperature controlling system, and a precisely controlled gas flow system. Gases pulses with concentration of 200 ppm balanced by dry air were introduced in the chamber under 1 atm of dry air background. Pure dry air was introduced between the pulses. Each of the analytes gases has the low humidity concentration about 2.2 × 10^{-6} (μmol/mol) and total hydrocarbon (THC) level is zero. The current is measured using a Keithley 2636A source measurement unit. All three produced similar results and the linear discriminant analysis (LDA) of each yielded points localized in approximately the same regions of parameter space for the three test gases. The results reported in this report were obtained in a long series of experiments from one of the devices.

RESULTS AND DISCUSSION

Current−voltage characteristics ($I-V$) in Figure 3a show the typical nonlinear Schottky-like transport behavior observed from the sensor elements at room temperature, necessary for a working e-nose. The electron transport characteristics are in general determined by the percolating conduction paths through the overlapping nanowires. The major features observed in the $I-V$ curves may be explained qualitatively with a simple core−shell model, similar to the well-known model of intergrain potential barrier.[21] For n−n junction, the electron has to pass at overlapping wires through the charge carrier depletion zones, because of the difference in electron concentration between bulk and the surface, formed at the interface of both nanowires. The potential barrier (V_s) is known to be strongly dependent upon the concentration of adsorbed oxygen, according to the following equation

$$n_s = N_d \exp\left(-\frac{eV_s}{k_B T}\right)$$

where n_s is surface electron concentration and N_d is the density of donors. k_b, T, and e are the Boltzmann constant, temperature, and charge on the electron, respectively. Thus, a symmetric nonlinear Schottky behavior for the n−n junction is shown.

The potential barrier in the p−n junction is more complex and depends on the work function and band gap differences between the two materials forming the junction, as well as the presence of eventual surface states, as shown in Figure 3b. The energy band diagram of the p−n junction between CuO (E_g = 1.35 eV) and ZnO (E_g = 3.32 eV), by considering the work functions (ϕ), electron affinity (χ) of both materials, is also shown in Figure 3b. The discontinuities (ΔE_c, ΔE_v) in the band edges at the interface results in different barrier heights for the two types of carrier, and hence the current through the overlapping nanowires consists of almost entirely of electrons under a forward bias of 1 V because the barrier for electrons is smaller than that for holes. The variation of the current with forward bias for the p−n junction is given by

$$I = A \exp\left(\frac{-eV_{s,p-n}}{k_B T}\right) \exp\left(\frac{eV}{k_B T}\right)$$

where $V_{s,p-n}$ is the barrier for the electrons.

By contrast, this model may not be suitable for explaining the $I-V$ characteristics of the p−p junction. Actually, the p−p junction exhibits near-linear $I-V$ characteristics at room temperature in Figure 3a. This implies that the holes, a majority carrier in p-type semiconductor, do not flow through the barrier height (if any). In p-type semiconductor, the adsorbed oxygens from the air create more holes available near the surface, forming the hole accumulation layer.[22] Thus, holes will flow through the layer and the transport characteristics will be determined by the thickness of the layer, not by height of the potential barrier, showing very weak rectifying behavior.

A representative set of source-drain currents, I_{SD}, measured as a function of time at an applied source-drain voltage of 1 V for Pd-decorated junction sensors at 250 °C is shows in Figure 4a−c. One of the three gases was periodically added to the continuously flowing air stream and then shut off. Representative values of the sensitivities of the sensor toward the gases are

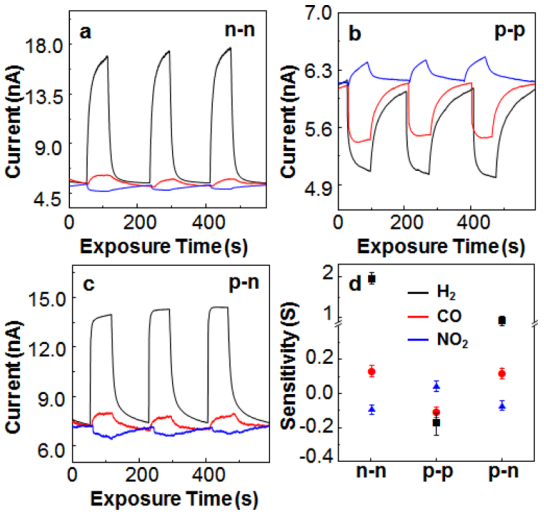

Figure 4. Representative set of I_{SD} measured as a function of time at an applied source-drain voltage of 1 V for Pd-decorated (a) n−n, (b) p−p, and (c) p−n junction. (d) Representative values of the sensitivities of the sensor toward the three gases. The sensitivity is defined as $S = (I_g - I_a)/I_a$, in which I_g and I_a are, respectively, the steady-state current values measured with the analyte gas added to the air stream and just the air stream alone.

given in Figure 4d. The sensitivity is defined as $S = (I_g - I_a)/I_a$, in which I_g and I_a are, respectively, the steady-state current values measured with the analyte gas added to the air stream and just the air stream alone. For n−n junction, adding each of the two reducing gases to the air stream causes the I_{SD} to increase in less than 1 min, returning to its initial value reversibly when the reducing gases are shut off. In contrast, NO_2 gas increases the I_{SD} when the nanowires are exposed to the gas. For H_2, CO, and NO_2, respectively, the measured S values on pristine nanowires at 250 °C, were 1.98, 0.15, and −0.15, with the analyte gas flow rate of 200 ppm.

The behavior of two reducing gases toward n−n junction was consistent with their reducing agents (i.e., as electron donors).[33,34] As reported previously, the high sensitivity toward H_2 is ascribed to the catalytic dissociation of diatomic hydrogen on the Pd nanoparticles and the spillover on to the nanowire's surface. Hydrogen atoms react with surface oxygen to create hydroxyl groups (OH^-). In the presence of a great deal of H atoms, these hydroxyls can further react with H to create water. At high temperature, this water can desorb to leave behind an oxygen vacancy, increasing the conductivity of the oxides.[32,35] Pd also provides sites at which CO is oxidized to form CO_2. The reactions will reduce the oxide from molecule-to-nanowire electron donation, and thus, the electrons are returned to the interface of the overlapping nanowires, resulting in a decrease of the potential barrier and the resistance of the sensor. On the contrary, the oxidizing gas (NO_2) provides additional oxygen to the oxide, increasing the upward band bending at the surface region, leading to the increase of the resistance of the sensor.[36]

When p−p junction sensor was exposed to the three gases, it gives the responses exactly in the opposite direction, compared with those in n−n junction, although the sensitivities are low (−0.2, −0.11, and 0.06 for the H_2, CO, and NO_2, respectively). In just the air stream alone, electrons are trapped by the adsorbed oxygen, leaving more holes available near the surface. As mentioned, the resistance is dependent on the thickness of the hole accumulation layer. When exposed to reducing gases, the chemisorptions reducing gases will deplete holes near the surface and reduce the thickness of the layer, resulting in an increase of resistance. The change in energy band diagram of n−n and p−p junction when exposed to the gases is described in Figure S2 (see the Supporting Information), respectively.

It was found the sensor responses of p−n junction toward three gases similar to those observed in the n−n junction sensor. However, the chemisorption process of the analytes in the p−n junction, which primarily occurs on the interface of the heterocontact, and on the surface of CuO and ZnO, may involve two or more processes. One process is likely the decrease in the barrier height because of the increase in the electron concentration from molecule-to-nanowire electron donation. In general, it is estimated that the electron concentration in ZnO is much higher than the hole concentration in CuO due to the presence of native defects acting as donors such as oxygen vacancies in metal-oxides.[37] Thus, the adsorbate induced shifts of the Fermi-level are domiant for CuO materials, which decreases the potential barrier height and decrease the resistance of the sensor. The other is likely the decrease of the thickness in the hole accumulation layer at the p-side due to the decrease of oxygen concentration at the surface of CuO, which increases the resistance. Such two competing effects should be considered for explaining the current response of the sensor. Actually, our results show that the sensitivities (0.94 and 0.11) of p−n junction toward H_2 and CO gases are lower than those (1.98 and 0.15) of n−n junction. The sensitivity of NO_2 was also decreased from −0.15 to −0.08.

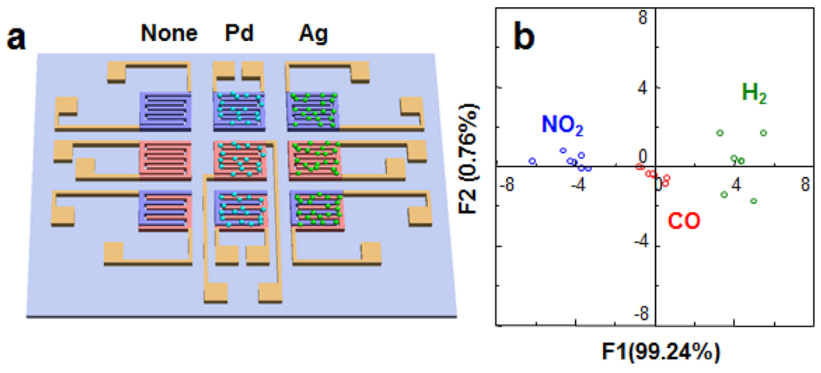

Figure 5. (a) Schematic illustration of 3 × 3 sensor arrays and results of an LDA analysis of the sensitivities obtained for the sensor array. (b) LDA analysis classified and separated the points corresponding to the various gases at 95% confidence level.

dx.doi.org/10.1021/am401635e | ACS Appl. Mater. Interfaces 2013, 5, 6802−6807

Figure S3 in the Supporting Information shows radar charts of gas sensitivity toward H_2, CO, and NO_2 gas species measured from the 9 sensor elements of the e-nose shown in Figure 5a. The sensitivities of n−n and p−n junction sensors toward the three gases give the response exactly in the opposite direction, compared with those in p−p junction sensor. The sensitivities of n−n junction sensor are higher than those of the p−n junction sensors. The response toward H_2 gas is overall high, especially with the n−n junction sensors decorated with Pd and Ag, whereas that toward NO_2 gas is relatively low, probably due to high oxygen partial pressure. Note that each gas sensor in the e-nose has its specific sensitivity pattern for different gas molecules, offering the function of discriminating various gas species. The aggregate data set for the e-nose was processed using LDA and plotted as two-dimensional maps to indicate the extent to which the analysis could separate the response of the e-nose to the three gases into separate classes, as shown in Figure 5b. LDA analysis was carried out using a commercial code (xlSTAT 2012, Addinsoft, France). The e-nose responses that we obtained produce the feature clusters among the three gases at 95% confidence level. That is, the three gases, H_2, CO, and NO_2, would be identified unequivocally by the e-nose described here, in gaseous samples each containing one of the three test gases mixed in air.

CONCLUSIONS

In conclusion, we describe a strategy for creating an air-bridge-structured percolating nanowire array platform that capable of promptly detecting and reliably discriminating between three gases (H_2, CO, and NO_2). Air-bridge-structured, which has the contact point between nanowire, alternatively driven multiple nanowires, which were made by metal deposition (by e-beam evaporator) and post annealing process in nanoscale on single substrate, was used to form two-dimensional microarray. The current transport characteristics are determined by the conduction paths through the overlapping nanowires. In n-n junction, the current, known as the thermionic emission current, has to pass the overlapping nanowires over the barrier height due to the depletion zone, whereas in p−p junction, the hole will pass through the hole accumulation layer in air. In the p−n junction, the electrons also flow over the barrier height, however, the resistance of the sensor also depends on the chemical reaction of the analytes on the surface of CuO, which decrease the sensitivities of the gases. These provide the ability of a given sensor array to differentiate among the junctions. The sensors were tested for their ability to distinguish three gases (H_2, CO, and NO_2), which they were able to do unequivocally when the data was classified using LDA.

Although several strategies for creating an e-nose have been suggested earlier, such as gradients in temperature, nanowire thickness and density, and variation of materials, forming the nanowire junctions array can be used to differentiate the sensor properties of the nanowire-based arrays. Other than the synthesis of the nanowires, all other steps in the fabrication of the e-nose were carried out using top-down microfabrication process, useful for making low cost, nanowire-based e-nose chips, useful for the for a variety of commercial industries, including the food, environmental, biomedical, and various scientific research fields. As future work, because the e-nose here was carried out by means of artificial gases, a robust sensing study will be carried out with real gas samples for real-world gas comparison test.[38]

ASSOCIATED CONTENT

Supporting Information

Figure giving an SEM images and the corresponding diameter distributions of ZnO and CuO nanowires, Energy band diagram of n−n and p−p junction sensors when they are exposed to the reducing gases and oxidizing gases, and Radar charts of gas sensitivity toward H_2, CO, and NO_2 gas species measured from the 9 sensor elements of the e-nose. This material is available free of charge via the Internet at http://pubs.acs.org/.

AUTHOR INFORMATION

Corresponding Author

*E-mail: jmbaik97@gmail.com.

Notes

The authors declare no competing financial interest.

ACKNOWLEDGMENTS

This research was supported by the Basic Science Program through the National Research Foundation of Korea (NRF) funded by the Ministry of Education, Science and Technology (2012-0002068 and 2012R1A1A1044091). We are very thankful to Professor Martin Moskovits (UCSB) for fruitful discussions.

REFERENCES

(1) Huang, M. H.; Mao, S.; Feick, H.; Yan, H.; Wu, Y.; Kind, H.; Weber, E.; Russo, R.; Yang, P. *Science* **2001**, *292*, 1897−1899.
(2) Huynh, W. U.; Dittmer, J. J.; Alivisatos, A. P. *Science* **2002**, *295*, 2425−2427.
(3) Comini, E.; Faglia, G.; Sberveglieri, G.; Pan, Z.; Wang, Z. L. *Appl. Phys. Lett.* **2002**, *81*, 1869−1871.
(4) Baughman, R. H.; Zakhidov, A. A.; de Heer, W. A. *Science* **2002**, *297*, 787−792.
(5) Sysoev, V. V.; Goschnick, J.; Schneider, T.; Strelcov, E.; Kolmakov, A. *Nano Lett.* **2007**, *7*, 3182−3188.
(6) McAlpine, M. C.; Ahmad, H.; Wang, D.; Heath, J. R. *Nat. Mater.* **2007**, *6*, 379−384.
(7) Yu, C.; Hao, Q.; Saha, S.; Shi, L.; Kong, X.; Wang, Z. L. *Appl. Phys. Lett.* **2005**, *86*, 063101−063101−3.
(8) Meier, D. C.; Semancik, S.; Button, B.; Strelcov, E.; Kolmakov, A. *Appl. Phys. Lett.* **2007**, *91*, 063118−063118−3.
(9) Hwang, S.; Kwon, H.; Chhajed, S.; Byon, J. W.; Baik, J. M.; Im, J.; Oh, S. H.; Jang, H. W.; Yoon, S. J.; Kim, J. K. *Analyst* **2013**, *138*, 443−450.
(10) Star, A.; Joshi, V.; Skarupo, S.; Thomas, D.; Gabriel, J.-C. P. *J. Phys. Chem. B* **2006**, *110*, 21014−21020.
(11) Aygun, S. M. Gas sensors based on ceramic p-n heterocontacts. M. Sc. Thesis, Iowa State University: Ames, IA, 2005.
(12) Chen, Y.; Yu, L.; Feng, D.; Zhuo, M.; Zhang, M.; Zhang, E.; Xu, Z.; Li, Q.; Wang, T. *Sens. Actuators, B* **2012**, *166−167*, 61−67.
(13) Sysoev, V.; Schneider, T.; Goschnick, J.; Kiselev, I.; Habicht, W.; Hahn, H.; Strelcov, E.; Kolmakov, A. *Sens. Actuators, B.* **2009**, *139*, 699−703.
(14) Li, D.; Hu, J.; Wu, R.; Lu, J. G. *Nanotechnology* **2010**, *21* (48), 485502.
(15) Chen, J.; Wang, K.; Hartman, L.; Zhou, W. *J. Phys. Chem. C* **2008**, *112*, 16017−16021.
(16) Hoa, N. D.; Van Quy, N.; Jung, H.; Kim, D.; Kim, H.; Hong, S.-K. *Sens. Actuators, B.* **2010**, *146*, 266−272.
(17) Liao, L.; Zhang, Z.; Yan, B.; Zheng, Z.; Bao, Q.; Wu, T.; Li, C.; Shen, Z.; Zhang, J.; Gong, H. *Nanotechnology* **2009**, *20*, 085203.
(18) Bedi, R. K.; Singh, I. *ACS Appl. Mater. Interfaces* **2010**, *2*, 1361−1368.
(19) Wang, C.; Fu, X.; Xue, X.; Wang, Y.; Wang, T. *Nanotechnology* **2007**, *18*, 145506.

(20) Hoa, N. D.; An, S. Y.; Dung, N. Q.; Van Quy, N.; Kim, D. *Sens. Actuators, B.* **2010**, *146*, 239−244.
(21) Fan, Z.; Ho, J. C.; Takahashi, T.; Yerushalmi, R.; Takei, K.; Ford, A. C.; Chueh, Y. L.; Javey, A. *Adv. Mater.* **2009**, *21*, 3730−3743.
(22) Talin, A. A.; Hunter, L. L.; Léonard, F.; Rokad, B. *Appl. Phys. Lett.* **2006**, *89*, 153102−153102−3.
(23) Lupan, O.; Ursaki, V.; Chai, G.; Chow, L.; Emelchenko, G.; Tiginyanu, I.; Gruzintsev, A.; Redkin, A. *Sens. Actuators, B.* **2010**, *144*, 56−66.
(24) Fujii, H.; Kanemaru, S.; Matsukawa, T.; Itoh, J. *Appl. Phys. Lett.* **1999**, *75*, 3986−3988.
(25) Fujii, H.; Kanemaru, S.; Matsukawa, T.; Itoh, J. *Jpn. J. Appl. Phys.* **1999**, *38*, 7237−7240.
(26) Ahn, M.-W.; Park, K.-S.; Heo, J.-H.; Park, J.-G.; Kim, D.-W.; Choi, K.; Lee, J.-H.; Hong, S.-H. *Appl. Phys. Lett.* **2008**, *93*, 263103−263103−3.
(27) Ahn, M.-W.; Park, K.-S.; Heo, J.-H.; Kim, D.-W.; Choi, K.; Park, J.-G. *Sens. Actuators, B.* **2009**, *138*, 168−173.
(28) Thong, L. V.; Loan, L. T. N.; Van Hieu, N. *Sens. Actuators, B* **2010**, *150*, 112−119.
(29) Dovgolevsky, E.; Konvalina, G.; Tisch, U.; Haick, H. *J. Phys. Chem. C* **2010**, *114*, 14042−14049.
(30) Zilberman, Y.; Tisch, U.; Shuster, G.; Pisula, W.; Feng, X.; Müllen, K.; Haick, H. *Adv. Mater.* **2010**, *22*, 4317−4320.
(31) Konvalina, G.; Haick, H. *ACS Appl. Mater. Interfaces* **2011**, *4*, 317−325.
(32) Paska, Y.; Stelzner, T.; Christiansen, S.; Haick, H. *ACS nano* **2011**, *5*, 5620−5626.
(33) Lupan, O.; Chai, G.; Chow, L. *Micro. Eng.* **2008**, *85*, 2220−2225.
(34) Chang, S.-J.; Hsueh, T.-J.; Chen, I.-C.; Huang, B.-R. *Nanotechnology* **2008**, *19*, 175502.
(35) Mubeen, S.; Moskovits, M. *Adv. Mater.* **2011**, *23*, 2306−2312.
(36) Choi, Y.-J.; Hwang, I.-S.; Park, J.-G.; Choi, K. J.; Park, J.-H.; Lee, J.-H. *Nanotechnology* **2008**, *19*, 095508.
(37) Yoon, D. H.; Yu, J. H.; Choi, G. M. *Sens. Actuators, B.* **1998**, *46*, 15−23.
(38) Tisch, U.; Haick, H. *MRS Bull.* **2010**, *35*, 797.